Journal of Catalysis 263 (2009) 220–227

Contents lists available at ScienceDirect

Journal of Catalysis

www.elsevier.com/locate/jcat

Comparative study of the kinetics of methane steam reforming on supported Ni and Sn/Ni alloy catalysts: The impact of the formation of Ni alloy on chemistry

Eranda Nikolla, Johannes Schwank, Suljo Linic *

Department of Chemical Engineering, 2300 Hayward Street, University of Michigan, Ann Arbor, MI 48109, USA

ARTICLE INFO

Article history:
Received 23 December 2008
Revised 8 February 2009
Accepted 9 February 2009
Available online 5 March 2009

Keywords:
SOFC
DFT
Steam reforming kinetics
Carbon deactivation
Ni alloys
Isotopic labeling

ABSTRACT

We report the results of detailed kinetic studies for methane steam reforming on supported Ni and Sn/Ni surface alloy catalysts. The kinetic data were interpreted in terms of mechanism-based overall rate expression. We show that the activation of C–H bonds in methane is the rate-controlling step on both catalysts. Isotopic CH_4/CD_4 labeling studies were performed to independently verify the proposed mechanism. The role of Sn is to displace Ni atoms from under-coordinated sites on Ni particles and to move the critical reaction channels to more abundant well-coordinated sites. We show that previously observed increased resistance to carbon deactivation of Sn/Ni compared to monometallic Ni in hydrocarbon reforming reactions can be attributed to the Sn-induced lowering in the binding energy of carbon on low-coordinate sites, which serve as carbon nucleation centers, and to an enhanced propensity of Sn/Ni to oxidize carbon surface species. The conclusions derived from the experimental studies are in agreement with DFT calculations.

1. Introduction

Steam reforming of hydrocarbons (for example methane, $CH_4 + H_2O \leftrightarrow CO + 3H_2$) is a crucial reaction for the production of synthesis gas. The process is also important for the direct electrochemical conversion of hydrocarbons in solid oxide fuel cells (SOFCs). Commercial catalyst for this reaction is Ni supported on an oxide. The process is run under a wide range of conditions with operating temperatures from ~750 to 1200 K. One of critical problems with long-term performance of Ni catalysts is the formation of carbon deposits on the catalyst surface, which evolve into carbon filaments, ultimately diminishing the performance of the catalyst [1–9].

It has been shown previously that the tolerance of Ni catalysts and electro-catalysts to carbon-induced deactivation in hydrocarbon steam reforming, partial oxidation, and electro-chemical oxidation reactions can be significantly improved by impregnating Ni with small amounts of Sn (2–1 wt% with respect to Ni for Ni particles with the diameter between 30 and 200 nm) [10–15]. For example, we have demonstrated that supported monometallic Ni catalysts deactivate rapidly in steam reforming of isooctane at stoichiometric steam to carbon ratio (see Fig. 8 in Ref. [11]). Similar conclusions were obtained for methane steam reforming at sub-stoichiometric steam to carbon ratios (see Fig. 7 in Ref. [11]). Sn/Ni catalysts showed significantly improved carbon tolerance compared to the monometallic Ni catalysts under identical experimental conditions [10–12].

While comprehensive kinetic studies on Sn/Ni catalysts have not been performed to date, it has been proposed, based on Density Functional Theory (DFT) calculations, that there are two likely mechanisms associated with the superior performance of Sn/Ni [10–12]. One mechanism is based on the kinetic control of the chemistry of carbon atoms and CH_x on the catalysts surface. This mechanisms assumes that the difference in the rates of the oxidation of carbon atoms and CH_x fragments and the rates associated with the formation of C–C bonds, which are critical for the development of solid carbon deposits that deactivate the catalyst, is significantly higher on Sn/Ni compared to Ni, i.e., the Sn/Ni catalyst is more efficient than Ni in the preferential formation of C–O rather than C–C bonds. The second mechanism assumes that carbon deactivation is governed by the thermodynamic control of the nucleation of carbon at the low coordinated Ni sites. Previous in-situ transmission electron studies (TEM) have demonstrated the importance of the low coordinated sites for nucleation and growth of carbon fibers [5,16]. This mechanism assumes that Sn atoms displace low-coordinated Ni atoms, preventing the nucleation of carbon deposits on these sites.

In this contribution we report the results of detailed kinetic studies for methane steam reforming on supported Sn/Ni and Ni catalysts. We focus on the analysis of the reaction kinetics at high temperatures (973–1073 K). These conditions are important for tubular methane steam reformer reactors and SOFCs [2]. The ki-

* Corresponding author. Fax: +1 734 764 7453.
E-mail address: linic@umich.edu (S. Linic).

0021-9517/$ – see front matter
doi:10.1016/j.jcat.2009.02.006

netic data for supported Ni and Sn/Ni catalysts were interpreted in terms of the mechanism-based overall rate expressions. Isotopic CH_4/CD_4 labeling studies were performed to further investigate the proposed catalytic sequence. These studies allowed us to independently identify the rate-controlling elementary steps on the different catalysts. The results of the kinetic studies were used to draw conclusions about the mechanisms responsible for the improved carbon tolerance of Sn/Ni compared to monometallic Ni. The conclusions of the experimental studies are supported by DFT calculations.

The kinetics of methane steam reforming on supported monometallic Ni catalysts have been studied by multiple researchers [9,17–23]. Although there have been many controversies, recent theoretical and experimental contributions have shown some consistent results. For example, Bengaard et al. utilized a combined theoretical and experimental approach to propose a mechanism for steam reforming of methane on Ni [9]. It was shown that methane steam reforming is a structure sensitive reaction and that under-coordinated Ni surface sites are more active than close packed Ni sites. It was also demonstrated that the rate-limiting step in the process is the activation of C–H bonds in methane. These conclusions are consistent with the recent experimental analysis of methane steam reforming at temperatures of 823–1023 K on Ni/MgO catalysts by Wei and Iglesia [20]. These authors also demonstrated that the forward rate is first order with respect to the methane partial pressure and that it does not depend on the partial pressure of water or the reaction products. It was also argued that the rates of carbon filament formation are governed by the chemical activity of carbon atoms chemisorbed on the catalyst surface. Previous contributions have postulated that for lower operating temperatures there is a switch in the rate-controlling step from the activation of CH_4 to the formation of CO on the catalyst surface [24].

2. Experimental methods and catalyst characterization

The Ni and the Sn/Ni catalysts were supported on (8 mol%) yttria-stabilized zirconia (YSZ). YSZ was prepared via a standard co-precipitation method. A mixture of yttrium nitrate ($Y(NO_3)_3\cdot 6H_2O$) and zirconyl chloride ($ZrOCl_2\cdot 2H_2O$) dissolved in deionized water was precipitated using a solution of ammonium hydroxide. After filtration and drying for 12 h, the precipitate was calcined at 1073 K for 2 h. Aqueous solutions of Ni nitrate were used to impregnate the YSZ support via the incipient wetness technique. The nominal Ni loading was about 15 wt% with respect to the total catalyst. After impregnation the catalysts were calcined at 873 K for 2 h in dry air to convert the Ni nitrate to Ni oxide and then reduced at 1173 K for 3 h in a stream of 30% H_2/N_2. The Sn/Ni/YSZ catalyst was synthesized by impregnating the NiO/YSZ catalyst with aqueous solution of Sn chloride ($SnCl_2\cdot 4H_2O$) via the incipient wetness technique. The nominal Sn loading was about 1 wt% with respect to the Ni content in the catalyst. The Sn/Ni/YSZ catalyst was also reduced at 1173 K for 3 h in a stream of 30% H_2/N_2.

Single point BET analysis was utilized to measure the surface area of the YSZ support via N_2 physisorption. The physisorption experiments were conducted using Quatachome's ChemBet 3000 equipped with thermal conductivity detectors (TCD). The active surface area and dispersion of the Ni and Sn/Ni crystallites was measured using H_2 chemisorption at 313 K. The measurements were conducted using Micromeritics ASAP 2020 instrument. Prior to hydrogen chemisorption the samples were reduced under hydrogen for 2 h at 1073 K ex situ and for 1 h at 1073 K in situ. The particle diameter and dispersion were calculated assuming a stoichiometry of one hydrogen atom per one Ni atom and spherical Ni particle geometry. These experiments yielded the crystallite size of approximately 50 nm for Ni and Sn/Ni samples. The crystallite size was independently verified using transmission electron microscopy (TEM) and X-ray diffraction (XRD). The TEM experiments were performed with the Joel 2010F electron microscope at 200 keV under a pressure of 1.5×10^{-7} Torr. Ni and Sn/Ni particles were detected using energy X-ray dispersive spectroscopy. The size of the crystallites was measured using Digital Micrograph. The XRD experiments were conducted using a Cu-$K\alpha$ source of a Philips XRG5000 3 kW X-ray generator with crystal alignment stage and a Rigaku thin film camera. The spectra were analyzed using the Scherrer equation with Jade v.7 software.

It was established based on quantitative analysis of X-ray photo-electron spectroscopy (XPS) results that for this Sn loading and the size of active particles the Sn concentration in the surface layers of Ni was between 15 and 20% [11]. Assuming that Sn and Ni atoms are homogeneously distributed among different particles, these results suggested that Sn almost exclusively segregates to the surface layers of Ni crystallites. To ensure that Sn and Ni atoms are in contact with each other in the Sn/Ni crystallites, we measured the near edge electronic structure of Sn/Ni, showing that chemical bonds between Sn and Ni atoms are formed in the surface layers of the particles [25]. Temperature programmed reduction (TPR) experiments showed that pure Ni and Sn materials reduce at ~700 and 900 K respectively, which is below the temperatures at which our experiments were performed [11,12]. The Sn/Ni catalysts reduced at ~670 K [11,12]. These measurements suggested that the catalytic materials used in these experiments are not expected to be oxidized under the reducing reaction conditions.

Kinetic studies were conducted isothermally in a packed bed quartz reactor operated at methane conversion from 2 to 10%. The diameter of the quartz reactor was 0.375 inches. The set-up included a set of mass flow controllers, a pair of thermocouples (inside and outside the reactor), and a syringe pump for water delivery. The steam lines were heated to 473 K to avoid condensation. The reactor effluent was analyzed using a Varian gas chromatograph (Varian CP 3800) equipped with thermal conductivity detectors (TCD) and a flame ionization detector (FID). Approximately 0.01 g of Ni/YSZ and Sn/Ni/YSZ catalysts with grain sizes of 150–200 μm were diluted with 0.5 g of quartz powder (250–400 μm) and loaded into the packed bed reactor. The bed height was ~0.5 cm. The catalyst powder was held in place by quartz wool plugs. The catalysts were reduced at 1173 K under a stream of 30% H_2/N_2 for 3 h prior to measuring reaction rates. The rates of methane steam reforming were measured at total flow rates of 50–200 sccm as temperature was varied from 923 to 1073 K for Ni and 973 to 1123 K for Sn/Ni.

Thermal gravimetric analysis (TGA) was performed using a TA instruments thermo-gravimetric analyzer (TGA Q500). Approximately 0.2 g of catalyst was reduced under 30% H_2/N_2 at 1073 K for 2 h. Once reduced, the catalysts were cooled to room temperature while exposed to pure nitrogen. The catalysts were then exposed to dry methane and the temperature was ramped to 1073 K at a set heating rate to measure the rate of methane decomposition. The weight of the sample was measured as a function of temperature to determine the amount of deposited carbon.

The Dacapo pseudo-potentials plane wave code (http://www.camp.dtu.dk) was employed for all spin polarized Density Functional Theory (DFT) calculations. The Ni surface was modeled using two different model surfaces, Ni(111) and Ni(211). These model systems allowed us to explore two representative active sites; under-coordinated step-edge sites on the (211) surface and close packed sites on the (111) surface. Our approach was to find a set of computational parameters that ensured the convergence of the relative energies of various structures with respect to each other. The optimal lattice constant for Ni bulk was calculated to be 3.52 Å. For model systems with the (111) surface termination,

we used a 3×3 supercell with 4 layers of metal atoms. The calculations for the (211) surface termination were performed using slabs with 9 layers of metal in 1×3 supercells. The convergence for the (111) surface was obtained with 18 special Chadi–Cohen k-points to sample the Brillouin zone. For the (211) surface, we used Monkhorst–Pack mesh with a $3 \times 3 \times 1$ k-point grid to sample the Brillouin zone. Adsorbates were adsorbed on one side of a slab. Approximately 15 Å of vacuum separated the slabs, and a dipole-correction scheme was employed to electro statically decouple the slabs. Electron exchange correlation effects were described using the generalized gradient approximation (GGA) with the Perdew–Wang 91 (PW91) functional [26–28]. Vanderbilt pseudo-potentials were employed to describe core electrons [29]. The density of valence electrons was determined self-consistently by iterative diagonalization of Kohn–Sham Hamiltonian using Pulay mixing of densities. The plane wave basis set used to describe the one-electron states was cut off at 350 eV. An electronic temperature (k_bT) of 0.1 was utilized during calculations with the final results extrapolated to 0 K. In the geometry optimization calculations on the (111) surface termination, the two top substrate layers and adsorbates were allowed to relax. On the (211) termination, the top six substrate layers and adsorbates were allowed to relax. The calculations were assumed to be converged when the maximum force on every degree of freedom was smaller than 0.01 eV/Å.

To model the Sn/Ni surface alloy we have employed identical Ni(111) slabs with a number of Sn atoms, equivalent to 1/9 and 2/9 ML, displacing Ni atoms in the surface layer of Ni. As described above, we have previously established by X-ray photoelectron spectroscopy (XPS) and electron energy loss near edge spectroscopy (ELNES) that Sn preferentially segregates to the surface layers of Ni [10–12,25]. Furthermore, DFT calculations also showed that the model surface alloy structures, with Sn atoms displacing Ni atoms from the top Ni layer, have lower formation energies relative to Sn displacing Ni atoms from the Ni bulk, Sn adsorbing on the surface of Ni, or Sn assembling in segregated pure Sn phases [11,12].

The first-order transition states for one-atom diffusion were identified by probing the high-symmetry sites between reactant and product states. The diffusing atom was fixed in the x–y plane on these sites and it was allowed to relax in the z direction. Energies were calculated for all high symmetry sites (hollow, bridge, and on-top) and the potential energy surfaces were constructed. This procedure allowed us to identify the transition state geometries as those associated with the maximum energy states along the reaction coordinate and minimum with respect to other degrees of freedom [30–32]. The forces in these calculations were minimized to 0.01 eV/Å. Transition states for the activation of C–H bonds in CH_4 and for the formation of C–O and C–C bonds were identified using Climbing Nudged Elastic Band method [33–35]. The identity of the first-order transition states was validated by making sure that the forces acting on the system change sign as the systems moves through the transition state geometry. We have further validated the transition states by slightly changing the geometry of the transition state along the reaction coordinate towards the product or reactant geometry and allowing the system to fully relax into the respective product and reactant states [36].

3. Results and discussions

The steam reforming reaction is operated at fairly high temperatures, leading to large gradients in temperature and concentration within the catalyst bed. These gradients along with contributions due to significant rates of reverse reactions can compromise the kinetic information obtained in reactor studies over a range of temperature, flow rates, and partial pressures [20]. To obtain reliable and rigorous kinetic parameters it is important to establish that the measurements are performed in reactor systems free of mass transport and diffusion limitations and not compromised by reverse rates [20].

The overall reaction rate (rate_n) of a chemical reaction can be expressed in terms of forward reaction rate (rate_f) and the approach to equilibrium according to Eq. (1). The approach to equilibrium (η) can be calculated based on Eq. (2) as the product of partial pressures of the reaction products divided by the product of the partial pressures of reactants and divided by the equilibrium constant for the overall reaction. The approach to equilibrium in a packed bad reactor varies from zero at the reactor inlet (if only reactants are fed into the reactor) to some finite value less than one at the reactor outlet, and it can be manipulated by changing the flow rate, mass of the catalyst, temperature, and other factors that might impact the overall conversion. We have performed all our experiments under conditions that yielded an approach to equilibrium less than 0.01 at the reactor outlet. Equation (1) shows that if the approach to equilibrium (η) is much less than one, then the measured overall reaction rate (rate_n) is approximately equal to the forward reaction rate (rate_f). The forward reaction rate is required to obtain rigorous reaction orders and overall activation barriers.

$$\text{rate}_f = \frac{\text{rate}_n}{(1-\eta)}, \tag{1}$$

$$\eta = \frac{[H_2]^3[CO]}{[CH_4][H_2O]}\frac{1}{K_{eq}}. \tag{2}$$

Aside from ruling out possible artifacts in our measurements due to the influence of reverse rates, we have also eliminated artifacts due to mass transport limitations or possible catalyst deactivation during the measurements. To make sure that the catalysts were not deactivating or sintering during the experiments, we cycled the temperature between the high and low limits multiple times during the process and were able to reproduce consistent rates. The absence of external mass transport limitations was verified by measuring the reaction rate at constant space time (W/Fao, catalyst mass/molar flow rate) but changing the flow velocity. These measurements showed that there was no change in the rate and therefore no external mass transport limitations. We have also changed the size of Ni/YSZ particles and mixed these with various amounts of inert. In these experiments we observed linear measured rate as a function of the fraction of Ni/YSZ mixed in the inert. The linearity to this relationship indicated that there were no internal diffusion limitations. This procedure is similar to those employed recently in the contributions of Iglesia and coworkers and outlined previously by other contributors [20,37–40].

3.1. Reaction orders and activation barriers

The reaction orders with respect to methane and water for methane steam reforming on Sn/Ni/YSZ and Ni/YSZ were determined by measuring the response of the forward rate to a change in the respective partial pressures of CH_4 and H_2O while keeping everything else in the system constant. Figs. 1a and 1c show that there is a linear increase in the forward rate for both Ni and Sn/Ni catalysts as the partial pressure of methane is increased. In these experiments, the partial pressure of methane was varied from 0.2 to 0.6 atm, while the partial pressure of water was kept constant at 0.39 atm. The feed was balanced by argon to reach the total pressure of 1 atm. Figs. 1b and 1d show that the forward reaction rate is not affected by a change in the partial pressure of water from 0.2 to 0.6 atm for a constant methane partial pressure of 0.39 atm. The behavior was consistently observed over a temperature range between 973 and 1073 K for Ni/YSZ and 1013 and 1123 K for Sn/Ni/YSZ.

Our results also show that as we varied the methane conversion from 1 to 10% by changing the reactor temperature for a give

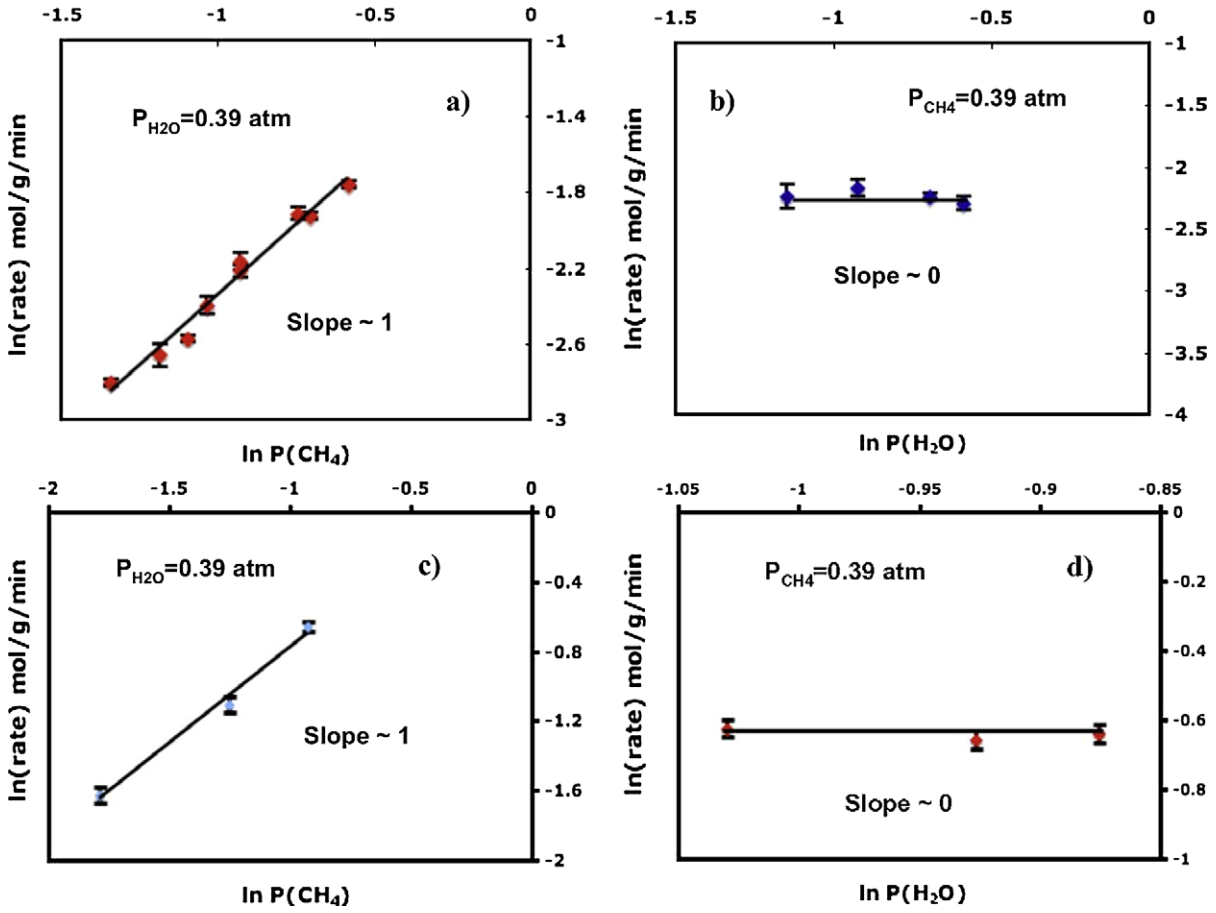

Fig. 1. (a) A plot of reaction rate as a function of the partial pressure of methane (P_{CH_4}) for a Sn/Ni/YSZ catalyst at 1073 K and a constant water partial pressure of 0.39 atm diluted in argon. Total pressure was 1 atm. (b) A plot of reaction rate as a function of P_{H_2O} for a Sn/Ni/YSZ catalyst at 1073 K and a constant methane partial pressure of 0.39 atm diluted in argon. Total pressure was 1 atm. (c) Same as in (a) for Ni/YSZ and at 1013 K. (d) Same as (b) for Ni/YSZ and at 1013 K.

flowrate, the order of the forward rate with respect to H_2O and CH_4 did not change on either catalyst. Since higher CH_4 conversion would lead to higher partial pressures of the reaction products, these observations imply that, for the conditions explored in this paper, the forward reaction rate is not sensitive to the changes in the partial pressure of the reaction products for either catalyst, and that the steady state coverage of product species (or surface intermediates which are precursors for the reaction products) on active sites does not change significantly. If this was not the case we would have seen a deviation in the reaction orders as a function of the change in conversion. Identical conclusions were made when small amount of product species were added to the inlet stream (up to 10 mol% with respect to methane). These conclusions are consistent with the results of our DFT calculations, which showed that at the relevant conditions ($T \sim 1000$ K) the adsorption energy of CO, H_2O, CO_2, and H_2 in its lowest energy configurations (e.g., dissociated or molecular) on under-coordinated sites of the Ni(211) surface are −164, −135, 19.2, and −77.2 kJ/mol, respectively. The adsorption energies are even lower for close packed Ni surfaces and for all sites on the Sn/Ni surfaces. These adsorption energies are insufficient to keep these species on the surface in significant concentrations under the high temperature conditions ($T > 973$ K), i.e. the Gibbs free energy of adsorption is positive. Based on the presented experimental results and the results of DFT calculations, we suggest that for both catalysts, the catalyst surface is approximately free of adsorbates under steady state conditions, and the overall rate is controlled only by the rate of the dissociation of CH_4. Similar observations were made previously for Ni/MgO catalysts [20].

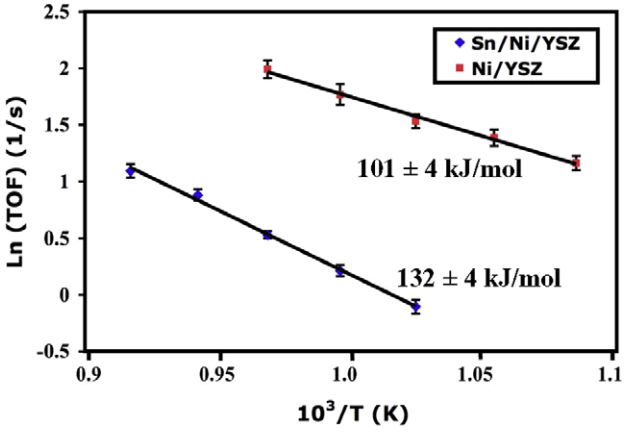

Fig. 2. A plot of the turnover frequency for methane steam reforming as a function of the inverse temperature for 1 wt% Sn/Ni/YSZ and Ni/YSZ catalysts when exposed to 0.39 atm of methane, 0.39 atm of water diluted in argon. The total pressure was 1 atm.

The apparent activation energy for methane steam reforming, defined in terms of the response of the forward rate to changes in operating temperature, was determined in an identical reactor setup. Prior to each measurement, the absence of mass transport limitations was verified. Fig. 2 shows an Arrhenius plot for methane steam reforming on the Ni/YSZ and Sn/Ni/YSZ catalysts for 0.39 atm of methane, 0.39 atm of water diluted in 0.22 atm of argon. We note that the reported TOFs for the Sn/Ni/YSZ catalyst were measured for the Sn loading of ∼1% and the particle

size of approximately 50 nm, which results in the Sn surface concentration between 15 and 20%. We find that as the loading of Sn increases the TOFs (reported with respect to the total number of surface Sn + Ni sites) decreases. The apparent activation barrier was determined to be $\sim 101 \pm 4$ and 132 ± 4 kJ/mol for the Ni and Sn/Ni catalysts, respectively. The measured turnover frequency and activation barrier on Ni is consistent with previous reports for supported Ni catalysts [20,22,41]. Further analysis of Fig. 2 suggests that the overall pre-exponential factor, calculated from the y-axis intercept in the Arrhenius plot, is by ~10–15 times larger for the Sn/Ni catalyst compared to the Ni catalyst. It is important to note that the overall pre-exponential factors were calculated from our experimental turnover frequencies based on the total number of surface sites, which are approximately identical for the Sn/Ni and Ni catalysts, i.e., it was not based on the number of active sites since it is almost impossible to count the active sites. This means that if the numbers of active surface sites (the sites that participate in the most frequent reaction channels) on Ni and Sn/Ni are different from each other, the overall pre-exponential factors will, in addition to describing the pre-exponential factor associated with the elementary step that controls the overall rate, also reflect this difference.

If one accepts that under the relevant conditions the surfaces of both catalysts are nearly free of adsorbates and that the rate is controlled by the dissociation of CH_4, then the difference in the overall activation barrier and pre-exponential factors between Ni and Sn/Ni is a consequence of the change in the nature of surface sites that dominate the catalytic process. It appears that on pure monometallic Ni the active sites (i.e., the sites responsible for the dominant reaction channel) are different in their chemical activity and relative abundance compared to the Sn/Ni alloy catalyst. We shed more light on this issue further below.

3.2. Thermal gravimetric analysis of methane activation

We have also utilized thermal gravimetric analysis (TGA) to study the decomposition of methane on the Ni and Sn/Ni catalysts. In these experiments, the change in weight of the catalyst exposed to 1 atm of dry methane was measured as the temperature was ramped from 298 to 1173 K. Fig. 3a shows a plot of the weight gain for the Sn/Ni/YSZ and Ni/YSZ catalysts as a function of temperature. The increase in the weight of the catalysts is a consequence of the formation of carbon deposits during methane decomposition (rxn 1).

$$CH_4 + {}^* \rightarrow C^* + 2H_2. \quad (1)$$

Fig. 3a shows that methane decomposes at lower temperature on Ni than on Sn/Ni. We have also plotted in Fig. 3b the measured rate of weight gain as a function of temperature, which is a measure of the rate of methane decomposition on the catalyst surface. Fig. 3b shows that the rate curve is broader on Sn/Ni compared to Ni. A possible interpretation for this is that there are multiple reaction channels (different sites) for methane decomposition on Sn/Ni. This supports the conclusions of our previous characterization studies which showed that in the Sn/Ni catalyst, the Sn atoms are dispersed in the surface layers of Ni particles forming a large number of geometrically and electronically diverse surface sites [10–12]. Careful inspection of Fig. 3b shows that for Sn/Ni there is a small shoulder in the rate curve, appearing at temperature just below 500 K, which overlaps with the peak of the rate curve for Ni. This suggests that there are a small number of sites on Sn/Ni that are similar to the sites on Ni in their ability to activate the C–H bonds in methane. However, the number of these sites is very small, and these sites are not responsible for the main methane decomposition channels, which are moved to higher temperatures for Sn/Ni compared to monometallic Ni.

We have also calculated, based on the measured rates of the decomposition of dry methane, the activation barriers for the dominating pathways, i.e., the pathways corresponding to the temperature where the rate reaches maximum values. To accomplish this we have employed the Redhead analysis [42]. If we assume that the rate of methane decomposition is first-order with respect to the partial pressure of methane and nth order with respect to the concentration of empty sites [*] we obtain the following decomposition rate expression:

$$\text{rate} = -\frac{d(^*)}{dt} = A_a P_{CH_4} [^*]^n \exp\left(\frac{-E_a}{RT}\right), \quad (3)$$

where A_a is the pre-exponential factor for adsorption of methane, P_{CH_4} is the partial pressure of methane, [*] is the concentration of the empty sites, E_a is the activation energy for methane dissociative adsorption, R is the gas constant, and T is the temperature. In our experiments temperature was varied linearly with time ($T = T_0 + \beta t$). Assuming that the maximum rate occurs at a temperature T_p when $\frac{dr}{dT} = 0$, we derive a relationship between the temperature associated with the maximum rate and the activation barrier associated with the reaction channel that yields the maximum rate:

$$A_a n [^*]^{n-1} P_{CH_4} \exp\left(\frac{-E_a}{RT_p}\right) = \frac{\beta E_a}{RT_p^2}. \quad (4)$$

If we assume that the pre-exponential factors for the dissociative adsorption step, the fraction of active sites that are empty at $T = T_p$, and the reaction order with respect to empty sites are identical for Ni and Sn/Ni, we find that the activation barrier for methane decomposition is higher by ~30 kJ/mol on Sn/Ni than on Ni. If we further assume that the maximum rate occurs at [*] = 0.5 (this is a reasonable assumption since it provides a compromise between the availability to free sites required for the activation of CH_4 and the high rate constant which depends on T), A_a is 10^5 1/s/atm for both catalysts (this assumption is based on an approximation of the translational, rotational and vibrational partition functions for the initial and transition states), and that the reaction order with respect to the concentration of empty sites n is 2 (two sites are required to activate methane), we obtain an activation barrier for methane decomposition of ~132 kJ/mol on Sn/Ni/YSZ and 103 kJ/mol on Ni/YSZ. We note that these activation barriers are not a strong function of n and [*], and similar activation barriers are obtained for significantly different values n and [*]. These activation barriers are almost identical to the activation barriers obtained in the Arrhenius analysis of the steady state reactor data shown in Fig. 2. The similarity in the measured activation barriers is not surprising, and it reinforces our conclusions that the rate of the overall process is governed by the activation of methane, and it is not sensitive to partial pressures of other gas-phase species.

3.3. DFT calculations of methane activation on Ni and Sn/Ni model systems

We have also utilized DFT calculations to study the dissociation of methane on Ni and Sn/Ni surface alloy. We have focused on two representative active sites, one containing closed packed terrace sites and another containing under-coordinated step/edge sites. To model the terrace and step/edge sites we have utilized the (111) and (211) surface termination, respectively. We calculated that the differences in the electronic energies between the activated complex (transition state) and the reactant in the methane dissociation reaction are 115, 105, and 79.5 kJ/mol on Sn/Ni(111), Ni(111) and Ni(211), respectively. The calculated geometries of transition states are shown in Fig. 4. The transition states geometries are very similar to those reported by Abild-Pedersen et al. in Ref. [43]. Previous

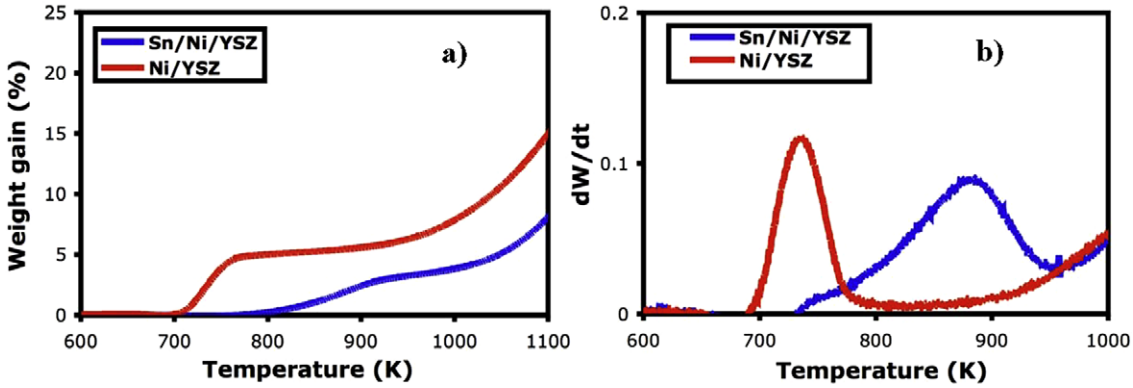

Fig. 3. (a) The percent weight gain of the catalyst as a function of temperature during methane decomposition on Sn/Ni/YSZ and Ni/YSZ catalysts. (b) The rate of methane decomposition as a function of temperature for Sn/Ni/YSZ and Ni/YSZ.

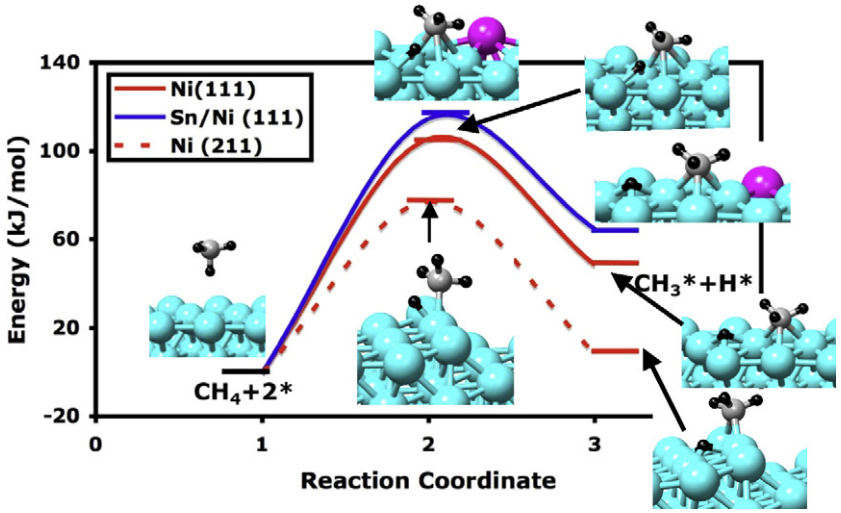

Fig. 4. Potential energy barriers for the activation of C–H bond in methane on Ni(211), Ni (111) and Sn/Ni (111). The inserts show the geometries of the initial, transition, and final states. The unit cell in the calculations was 3×3 for the (111) surface and 3×1 for the (211) surface. The concentration of Sn in the surface layer of Sn/Ni(111) was 1/9 ML. The Sn atom is in purple, H is black, Ni is light blue, and C is gray. (For interpretation of the references to color in this figure legend, the reader is referred to the web version of this article.)

calculations have reported the activation barriers for the dissociation of CH_4 on Ni(111) ranging between 70 and 125 kJ/mol [44–49]. It has also been reported that the difference between the barriers for methane activation on Ni(111) and Ni(211) is ~20 kJ/mol, which is close to our value of 25 kJ/mol. It can easily be shown that if we express the rate constant based on the transition state theory and evaluate the appropriate derivative of the rate constant to obtain the activation barrier, defined in terms of Arrhenius rate expressions as the parameter that describes the change in the rate constant due to the change in T, the calculated activation barriers for methane dissociation, defined in terms of Arrhenius rate expressions, at relevant temperatures are ~123, 113, and 87.5 kJ/mol for Sn/Ni(111), Ni(111), and Ni(211), respectively. The analysis suggests that the dissociation of CH_4 is more facile on low-coordinated Ni sites. Reasonable agreement between the measured overall activation barrier and calculated barrier on under-coordinated Ni sites argues that the dominant reaction channels on monometallic Ni involve the activation of CH_4 in the rate-controlling step on under-coordinated Ni sites. We note that similar observations have been made by others based on DFT calculations or by comparing the reaction rates on Ni particles with different concentrations of under-coordinates sites [24,43]. The DFT studies also suggest that on Sn/Ni the measured overall activation barrier associated with the dominant reaction channel is close to the barrier calculated for the dissociation of CH_4 on the Ni(111) and Sn/Ni(111) surfaces. The results suggest that Sn neutralizes the highly active under-coordinated sites on Ni and moves the dominant pathways to well-coordinated sites. This is consistent with the higher measured value of Arrhenius pre-exponential factor for Sn/Ni compared to monometallic Ni, which is a consequence of a larger number of well-coordinated than close packed sites on a catalytic particle. Similar conclusions have been made for sulfur modified Ni catalysts which also exhibit improved carbon tolerance compared to monometallic Ni [9].

3.4. CH_4/CD_4 kinetic isotope labeling studies

The analysis presented in the previous sections suggested that the rate controlling step in methane steam reforming on Ni and Sn/Ni is the activation of C–H bonds in methane. To independently verify our conclusions regarding the nature of the rate-controlling elementary step we have studied the kinetics of the process using labeled methane (CD_4). In these experiments, the reaction rates were measured in an identical differential reactor setup, free of mass transport limitations and artifacts due to reverse rates. Fig. 5 shows plots of the measured forward reaction rates as a function of time for Ni/YSZ and Sn/Ni/YSZ catalysts as the feed was switched from CH_4 to CD_4 and back to CH_4. Fig. 5 shows that as the feed is switched from CH_4 to CD_4, the forward rate decreases for both catalysts. Quantitative analysis of the reactions rates shows that the

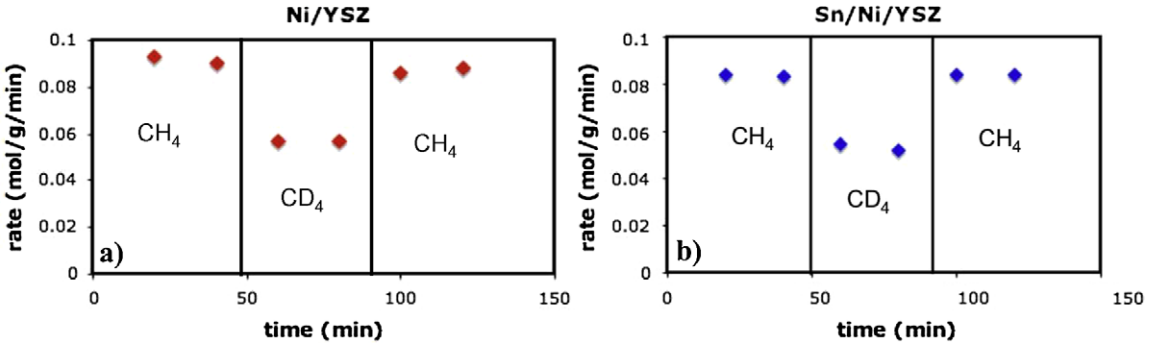

Fig. 5. The rate of steam reforming is measured for CH_4 and CD_4 reactants as a function of time on (a) Ni/YSZ at 973 K and (b) Sn/Ni/YSZ at 1033 K. The dark lines depict points in time when the reactant is switched from CH_4 to CD_4 and back to CH_4. The steam-to-carbon ratio was 1.

drop in forward rate is approximately equal on both catalysts for a given reaction temperature. The observed kinetic isotope effect demonstrates that the overall rate is controlled to a similar degree by the rate of C–H bond dissociation on both catalysts. Similar observations were made by others for supported monometallic Ni catalysts [20,50]. We note that the measured kinetic isotope effect of ~1.6 is slightly lower than the isotope effect predicted based on the transition state theory, assuming that the rate-controlling step involves the C–H and C–D vibration with a frequency identical to those measured in the gas-phase for CH_4 and CD_4, respectively. The reasons for this discrepancy might be in slightly different vibrational frequencies of normal modes involved in the reaction coordinate on two surfaces compared to the normal modes associated with gas-phase CH_4 and CD_4.

3.5. Mechanisms associated with the improved carbon-tolerance in reforming reactions of Sn/Ni compared to Ni

The kinetic studies allow also us to draw conclusions regarding the underlying mechanisms responsible for the improved carbon-tolerance of Sn/Ni compared to Ni. Our results show that Sn atoms cause the rate-controlling CH_4 activation step to move from low-coordinated Ni sites to the well-coordinated sites. This is consistent with our DFT calculations which showed that Sn preferentially displaces Ni atoms from the under-coordinated sites. The presence of the Sn atoms increases the activation barriers for the dissociation of CH_4. Furthermore, it also weakens the binding of the carbon atoms to the low-coordinated sites, which is a requirement for the nucleation of carbon at these sites. In very simple terms, the Sn atoms increase the chemical potential of carbon at the under-coordinated sites and decrease the thermodynamic driving force for the carbon atoms to approach these sites. This mechanism by which Sn improves the tolerance of the catalyst to the carbon-induced deactivation is very similar to the mechanism proposed previously for Au and S additives [9].

We also find that under the explored conditions (above 950 K) the formation of the CO adsorbate does not control the reaction rate on either catalyst. Based on the experimental results, we cannot rule out that the rate of formation of the C–C bonds (the kinetic control of the formation of carbon deposits described in the introduction section), which is a prerequisite for the formation of carbon fibers, is not affected by the formation of the surface alloy. To address this question we have calculated the maximum rates for the dissociation of CH_4, and the formation of the C–C and C–O bonds on the Ni and Sn/Ni model systems. The activation barriers for these processes were calculated in DFT calculations. In these calculations we have assumed that the activation of CH_4 on monometallic Ni takes place on low-coordinated sites of the (211) surface, while on Sn/Ni, the close-packed sites on the (111) surface are involved in the process. These assumptions are supported by the results of experimental analysis discussed in the preceding paragraphs. The calculated barriers for the activation of CH bonds in CH_4 are shown in Fig. 4. The activation barrier for the formation of C–O bonds was calculated as the energy difference between the highest and lowest points on the lowest potential energy surface associated with the diffusion of C and O atoms and the formation of the C–O bonds on the closed packed Ni(111) and Sn/Ni(111) surfaces. Similarly, the activation barrier for the formation of C–C bonds was calculated as the energy difference between the highest point and lowest point on the lowest potential energy surfaces associated with the diffusion of C atoms and the formation of C–C bonds on the identical surfaces. It is important to stress that the calculated activation barriers for the formation of C–O and C–C bonds are very similar to those associated with the formation of HC–O and HC–CH bonds respectively, which might be important if the CH fragment is the most abundant carbon containing adsorbate. The pre-exponential factors for these processes were approximated using the transition state theory to be 10^5 1/atm/s for the dissociative adsorption of CH_4 and 10^{13} 1/s for the formation of C–O and C–C bonds. In the rate calculations we have assumed that the concentration of reactants in a particular step is unity with respect to a standard state. This means that the obtained rate values for the formation of C–O and C–C bonds represent the upper bound since the coverage of surface intermediates in steam reforming of methane will be significantly lower than unity.

Based on the simple analysis in Fig. 6, it is clear that on monometallic Ni the maximum rates of C–C bond formation are higher than the rates of the C–O bond formation. This might be an important reason for the deactivation of the Ni catalyst by solid carbon deposits during hydrocarbon steam reforming at moderate steam to carbon ratios, i.e., moderate ratio of oxygen to carbon adsorbates on surface. It is also clear that on Sn/Ni the rate of C–C bond formation is lower than the rate of the C–O bond formation, which suggests that C atoms and CH_x fragments are preferentially oxidized on Sn/Ni. The reason for this is that the barrier for the diffusion of C atoms and CH_x fragments on Sn/Ni is significantly larger than on pure Ni surface. We find that as the concentration of Sn in the Ni surface layer is increased the activation barrier for the diffusion of carbon species increases dramatically due to repulsion between Sn and C atoms. For example, for an Sn surface concentration of 2/9 ML the impact on the rate of the C–C bond formation is dramatic as corroborated by the results shown in Fig. 6. This means that even a small number of Sn atoms dispersed in the top layer of Ni would affect the rate of carbon-induced deactivation significantly. This observation is in agreement with our experimental findings.

The analysis suggests that in addition to lowering the thermodynamic driving force associated with the nucleation of carbon on low-coordinated Ni sites, the Sn/Ni catalysts also enhance the rates of carbon removal by preferentially oxidizing carbon species rather than forming C–C bonds. Furthermore, the analysis in Fig. 6 also suggests that at high temperatures, consistent with the experi-

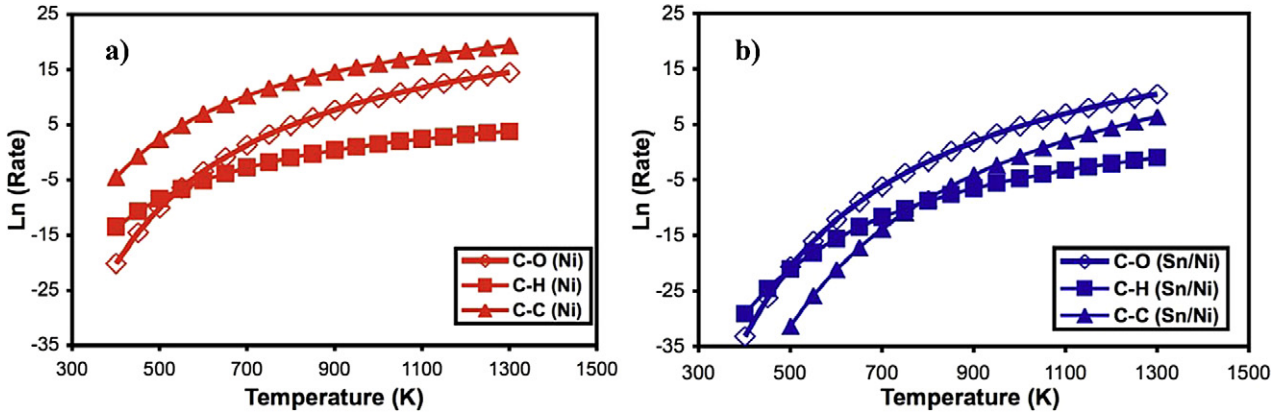

Fig. 6. Calculated maximum rates of C–H bond activation in methane, C–C bond formation, and C–O bond formation are plotted as a function of temperature for Ni and Sn/Ni surface alloy. It is assumed the C–H bond is activated on Ni(211) surface for Ni and on Sn/Ni(111) surface for Sn/Ni. The pre-exponential factor for this reaction is assumed to be 10^5 1/s. The activation barrier for the formation of C–O and C–C bonds was calculated as the energy difference between the highest and lowest points on the potential energy surfaces associated with the diffusion of C and O atoms and the formation of the C–O and C–C bonds respectively on the closed packed Ni (111) and Sn/Ni (111) surfaces. The pre-exponential factors for these reactions are assumed to be 10^{13} 1/s for both surfaces. The unit cell in the calculations was 3×3 for the (111) surface and 3×1 for the (211) surface. The concentration of Sn in the surface layer of Sn/Ni(111) was 2/9 ML.

ments performed herein, the rate-controlling step in the formation of products on both surfaces is the activation of C–H bonds in methane. We note that the rate controlling step is the step with a lower rate between the activation of C–H bond and the formation of C–O bond, i.e., the rate of C–C bonds cannot control the process since it leads to a dead end in the reaction. Fig. 6 also shows that at lower temperatures the rate-limiting step on both surfaces is the formation of C–O bonds as has been postulated previously [24].

4. Conclusion

A kinetic assessment of methane steam reforming on Sn/Ni/YSZ and Ni/YSZ catalysts is obtained using a combination of kinetic studies, isotopic-labeling experiments, and DFT calculations. We found that the reaction rate on Sn/Ni/YSZ and Ni/YSZ is first-order with respect to methane and it is independent of the water partial pressure. Furthermore, we established that C–H bond activation in methane is the rate-limiting step for both catalysts. We found that while on monometallic Ni the active sites are the under-coordinated Ni sites, on Sn/Ni the active sites are more abundant, well-coordinated terrace sites. The observed decrease in carbon deactivation of Sn/Ni was attributed to the Sn-induced lowering in the binding energy of carbon on low-coordinate sites, serving as carbon nucleation center and to an improved propensity of Sn/Ni to oxidize carbon atoms and fragments.

Acknowledgments

We gratefully acknowledge the support of the US Department of Energy DOE-BES, Division of Chemical Sciences (FG-02-05ER15686), NSF (CBET 0756255), ONR (N00014-08-1-0122), DOE-NETL (FC26-05-NT-42516) and National Automotive Center (NAC).

References

[1] C.M. Finnerty, N.J. Coe, R.H. Cunningham, R.M. Ormerod, Catal. Today 46 (1998) 137.
[2] J.R. Rostrup-Nielsen, in: Catalysis—Science and Technology, vol. 5, Springer, Berlin, 1984.
[3] J.R. Rostrup-Nielsen, J. Sehested, J.K. Norskov, Adv. Catal. 47 (2002) 65.
[4] J. Rostrup-Nielsen, J.K. Norskov, Top. Catal. 40 (2006) 45.
[5] F. Abild-Pedersen, J.K. Norskov, J.R. Rostrup-Nielsen, J. Sehested, S. Helveg, Phys. Rev. B (2006) 73.
[6] N.C. Triantafyllopoulos, S.G. Neophytides, J. Catal. 217 (2003) 324.
[7] T. Takeguchi, Y. Kani, T. Yano, R. Kikuchi, K. Eguchi, K. Tsujimoto, Y. Uchida, A. Ueno, K. Omoshiki, M. Aizawa, J. Power Sources 112 (2002) 588.
[8] J.R. Rostrupnielsen, L.J. Christiansen, Appl. Catal. A 126 (1995) 381.
[9] H.S. Bengaard, J.K. Norskov, J. Sehested, B.S. Clausen, L.P. Nielsen, A.M. Molenbroek, J.R. Rostrup-Nielsen, J. Catal. 209 (2002) 365.
[10] E. Nikolla, A. Holewinski, J. Schwank, S. Linic, J. Am. Chem. Soc. 128 (2006) 11354.
[11] E. Nikolla, J. Schwank, S. Linic, J. Catal. 250 (2007) 85.
[12] E. Nikolla, J. Schwank, S. Linic, Catal. Today 136 (2008) 243.
[13] D.L. Trimm, Catal. Today 49 (1999) 3.
[14] D.L. Trimm, Catal. Today 37 (1997) 233.
[15] C. Padeste, D.L. Trimm, R.N. Lamb, Catal. Lett. 17 (1993) 333.
[16] S. Helveg, C. Lopez-Cartes, J. Sehested, P.L. Hansen, B.S. Clausen, J.R. Rostrup-Nielsen, F. Abild-Pedersen, J.K. Norskov, Nature 427 (2004) 426.
[17] E. Achenbach, E. Riensche, J. Power Sources 52 (1994) 283.
[18] J.G. Xu, G.F. Froment, AIChE J. 35 (1989) 88.
[19] J.G. Xu, G.F. Froment, AIChE J. 35 (1989) 97.
[20] J.M. Wei, E. Iglesia, J. Catal. 224 (2004) 370.
[21] J.W. Snoeck, G.F. Froment, M. Fowles, Ind. Eng. Chem. Res. 41 (2002) 4252.
[22] K. Ahmed, K. Foger, Catal. Today 63 (2000) 479.
[23] P. Munster, H.J. Grabke, J. Catal. 72 (1981) 279.
[24] G. Jones, J.G. Jokobsen, S.S. Shim, M.P. Andersson, J. Rossmeisi, F. Abild-Pedersen, T. Bligaard, S. Helveg, B. Hinnemann, J.R. Rostrup-Nielsen, I. Chorkendorff, J. Sehested, J.K. Norskov, J. Catal. 259 (2008) 147.
[25] E. Nikolla, J. Schwank, S. Linic, J. Am. Chem. Soc. (2009), Article ASAP.
[26] J.P. Perdew, J.A. Chevary, S.H. Vosko, K.A. Jackson, M.R. Pederson, D.J. Singh, C. Fiolhais, Phys. Rev. B 46 (1992) 6671.
[27] J.P. Perdew, Y. Wang, Phys. Rev. B 46 (1992) 12947.
[28] J.P. Perdew, K. Burke, M. Ernzerhof, Chemical Applications of Density-Functional Theory 629 (1996) 453.
[29] D. Vanderbilt, Phys. Rev. B 41 (1990) 7892.
[30] S. Linic, J.W. Medlin, M.A. Barteau, Langmuir 18 (2002) 5197.
[31] S. Laursen, S. Linic, Phys. Rev. Lett. (2006) 97.
[32] M. Enever, S. Linic, K. Uffalussy, J.M. Vohs, M.A. Barteau, J. Phys. Chem. B 109 (2005) 2227.
[33] G. Henkelman, B.P. Uberuaga, H. Jonsson, J. Chem. Phys. 113 (2000) 9901.
[34] G. Mills, H. Jonsson, G.K. Schenter, Surf. Sci. 324 (1995) 305.
[35] S. Linic, M.A. Barteau, J. Am. Chem. Soc. 126 (2004) 8086.
[36] S. Linic, M.A. Barteau, J. Catal. 214 (2003) 200.
[37] H.S. Fogler, Elements of Chemical Reaction Engineering, 4th ed., Prentice–Hall, 2005.
[38] R.L. Augustine, Heterogeneous Catalysis for Synthetic Chemist, CRC Press, 1996.
[39] R.M. Koros, E.J. Nowak, Chem. Eng. Sci. 22 (1967) 470.
[40] R.J. Madon, M. Boudart, Ind. Eng. Chem. Fundam. 21 (1982) 438.
[41] S.B. Wang, G.Q. Lu, Energy Fuels 12 (1998) 1235.
[42] R.I. Masel, Principles of Adsorption and Reaction on Solid Surfaces, John Wiley & Sons, Inc., Canada, 1996.
[43] F. Abild-Pedersen, O. Lytken, J. Engbaek, G. Nielsen, I. Chorkendorff, J.K. Norskov, Surf. Sci. 590 (2005) 127.
[44] H. Burghgraef, A.P.J. Jansen, R.A. Vansanten, Surf. Sci. 324 (1995) 345.
[45] H. Burghgraef, A.P.J. Jansen, R.A. Vansanten, J. Chem. Phys. 101 (1994) 11012.
[46] H. Yang, J.L. Whitten, J. Chem. Phys. 96 (1992) 5529.
[47] H. Yang, J.L. Whitten, Surf. Sci. 255 (1991) 193.
[48] P.E.M. Siegbahn, I. Panas, Surf. Sci. 240 (1990) 37.
[49] P. Kratzer, B. Hammer, J.K. Norskov, J. Chem. Phys. 105 (1996) 5595.
[50] K. Otsuka, S. Kobayashi, S. Takenaka, J. Catal. 200 (2001) 4.